Journal of Alloys and Compounds 509 (2011) 6640–6643

Contents lists available at ScienceDirect

Journal of Alloys and Compounds

journal homepage: www.elsevier.com/locate/jallcom

Enhanced glass forming ability and refrigerant capacity of a $Gd_{55}Ni_{22}Mn_3Al_{20}$ bulk metallic glass

L. Xia[a,b], K.C. Chan[a,*], M.B. Tang[c]

[a] Department of Industrial and Systems Engineering, The Hong Kong Polytechnic University, Hung Hom, Hong Kong, China
[b] Institute of Materials, Shanghai University, Shanghai 200072, China
[c] Key Laboratory of Transparent and Opto-functional Inorganic Materials, Shanghai Institute of Ceramics, Chinese Academy of Sciences, Shanghai 200050, China

ARTICLE INFO

Article history:
Received 9 March 2011
Accepted 18 March 2011
Available online 29 March 2011

Keywords:
Bulk metallic glass
Glass forming ability
Magnetocaloric effect
Micro-alloying

ABSTRACT

In this work, a small amount of Mn was added to a $Gd_{55}Ni_{25}Al_{20}$ glass forming alloy, as a replacement for Ni, and a $Gd_{55}Ni_{22}Mn_3Al_{20}$ bulk metallic glass (BMG) was obtained by suction casting. Its glass forming ability (GFA) was characterized by X-ray diffraction and differential scanning calorimetry, and its magnetic properties were measured using a magnetic property measurement system. It is found that the minor Mn addition can significantly improve both the GFA and the magnetocaloric effect (MCE) of the alloy. The refrigerant capacity (*RC*) of the BMG can reach a high value of 825 J kg^{-1} under a field of 3979 kA/m, which is about 29% larger than that of a $Gd_{55}Ni_{25}Al_{20}$ BMG. The effect of the minor Mn addition on the GFA and MCE of the BMG was investigated in the study.

1. Introduction

Bulk metallic glasses (BMGs), as an emerging class of materials with unique disordered atomic configuration and excellent properties, have attracted intensive research interest over the past decades [1–5]. They have exhibited promising application potentials as advanced engineering materials in industry due to their ultrahigh strength up to 5 GPa for Co-based BMGs [6], 3 GPa for Ni-based BMGs [7] and 2 GPa for Zr–Cu-based BMGs [8–10] at room temperature. More recently, the excellent magnetocaloric effect (MCE) of BMGs have also evoked considerable research interest due to the potential as a class of functional materials in magnetic refrigeration technology [11–20]. The magnetic BMGs usually undergo second order magnetic transition with broadened magnetic entropy change (ΔS_m) peaks resulting in high values of refrigerant capacity (*RC*). They also exhibit some unique properties that are superior to those of crystalline alloys, such as: (i) soft magnetic properties with nearly zero magnetic hysteresis, (ii) large electric resistance, minimizing eddy current loss, (iii) high corrosion resistance and (iv) fine molding and processing behavior. These characteristics are technically important for the use of BMGs as magnetic refrigerants for Ericsson circulation [11–24].

Among the various magnetic BMGs, $Gd_{55}Ni_{25}Al_{20}$ ternary BMG has been shown to exhibit good glass forming ability (GFA) and excellent MCE [12]. Minor additions have been shown to be effective in improving the properties of BMGs [25,26]. In order to further enhance the GFA and MCE of $Gd_{55}Ni_{25}Al_{20}$ BMG, the minor addition of Mn as a replacement for Ni is adopted in the present investigation. A $Gd_{55}Ni_{22}Mn_3Al_{20}$ glassy rod is synthesized by the conventional copper mold suction casting method. The effect of the minor Mn addition on the GFA and MCE of $Gd_{55}Ni_{25}Al_{20}$ BMG is investigated.

2. Experimental

$Gd_{55}Ni_{25}Al_{20}$ and $Gd_{55}Ni_{22}Mn_3Al_{20}$ ingots were prepared by arc-melting 99.9% (at.%) pure Gd, Ni, Al and Mn under a titanium-gettered argon atmosphere. The as-cast rods, with diameters 2 mm, were prepared by copper mold suction casting in an argon atmosphere. The structure of the samples was characterized by X-ray diffraction (XRD) on a Rigaku D_{max}-2550 diffractometer using Cu Kα radiation. The thermal properties of the BMG were characterized by differential scanning calorimetry (DSC) carried out under a purified argon atmosphere in a Perkin-Elmer DIAMOND DSC at a heating rate of 20 K/min. The liquidus temperature of the samples was obtained from the high temperature DSC curve measured by a NETZSCH DSC 404C at a heating rate of 20 K/min. The magnetic properties of the BMG were measured from 10 K to 300 K by a Quantum Design Physical Properties Measurement System (PPMS 6000). The ΔS_m of the sample, subject to the magnetic field (H) variation in an isothermal process, was obtained by integrating over the whole magnetic field as follows:

$$\Delta S_m(T,H) = S_m(T,H) - S_m(T,0) = \int_0^H \left(\frac{\partial M}{\partial T}\right)_H dH \qquad (1)$$

where M is the magnetization of the sample under a magnetic field H, at a temperature T. The MCE of the BMG was studied by constructing the temperature dependence of ΔS_m from the isothermal magnetization curve. As the refrigeration capacity is regarded as a useful parameter when evaluating the MCE of refrigerant

* Corresponding author.
E-mail addresses: mfkcchan@inet.polyu.edu.hk, mfkcchan@polyu.edu.hk (K.C. Chan).

0925-8388/$ – see front matter © 2011 Elsevier B.V. All rights reserved.
doi:10.1016/j.jallcom.2011.03.120

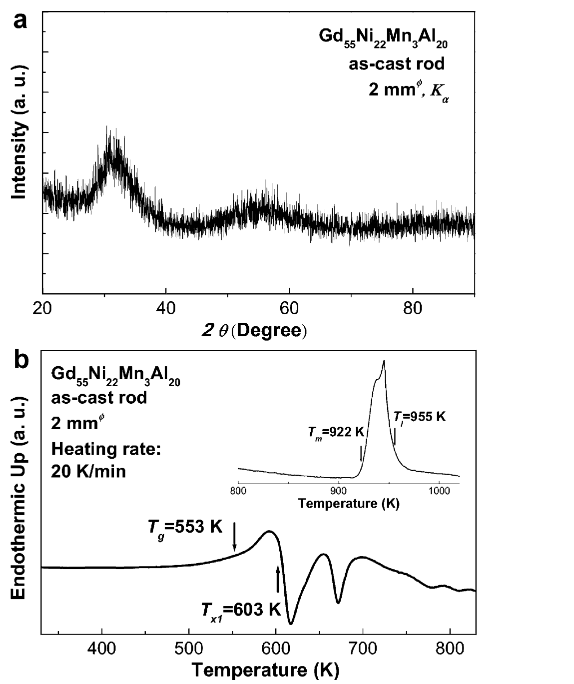

Fig. 1. (a) XRD pattern of $Gd_{55}Ni_{22}Mn_3Al_{20}$ as-cast rod; (b) the DSC trace of $Gd_{55}Ni_{22}Mn_3Al_{20}$ as-cast rod at a heating rate of 20 K/min, the inset the melting behavior of the rod.

materials for technological applications, the *RC* of the samples is also calculated as follows:

$$RC = -\Delta S_m^{peak} \times \Delta T_m \quad (2)$$

where ΔT_m is the temperature width at the half maximum of $-\Delta S_m^{peak}$.

3. Results and discussion

Fig. 1 shows the XRD pattern (a) and the DSC trace (b) of a $Gd_{55}Ni_{22}Mn_3Al_{20}$ as-cast rod, with a diameter of about 2 mm. The glassy characteristics of the as-cast rod are illustrated by the typical broad diffraction maxima of the amorphous phases in the XRD pattern, and the endothermic glass transition behavior before crystallization in the continuous DSC trace of the rod. The onset temperature of glass transition (T_g) at a heating rate of 20 K/min is about 553 K. Several exothermic crystallization reactions occur after the glass transition, and the onset temperature of the first step crystallization (T_{x1}) is about 603 K, at the same heating rate. The melting and liquidus temperatures (T_m and T_l) of the alloy are about 922 K and 955 K, as marked respectively on the high temperature DSC trace in the inset of Fig. 1(b). Thus, the supercooled liquid region ΔT and the reduced glass transition temperature T_{rg} (T_g/T_l) of the rod are about 50 K and 0.58, respectively. The parameter $\gamma(T_x/(T_g+T_l))$ of the $Gd_{55}Ni_{22}Mn_3Al_{20}$ BMG is about 0.40, and thus the critical cooling rate (R_c) and the section thickness (Z_c) of the BMG can be predicted to be about 22.4 K/s and 4.9 mm respectively. Compared to the values of a $Gd_{55}Ni_{25}Al_{20}$ BMG [12], it is found that minor Mn addition can definitely improve the ΔT, T_{rg}, γ and Z_c, leading to improvement of the GFA and thermal stability of the BMG.

Fig. 2 shows the hysteresis loops of the $Gd_{55}Ni_{22}Mn_3Al_{20}$ as-cast rod, measured at 10 K and 300 K, under a field of 1592 kA/m. For comparison purposes, the hysteresis loop of the $Gd_{55}Ni_{25}Al_{20}$ as-cast rod at 10 K is also illustrated in the figure. The $Gd_{55}Ni_{22}Mn_3Al_{20}$ glassy rod is ferromagnetic at 10 K and paramagnetic at room temperature. The saturation magnetization (M_s) of the as-cast $Gd_{55}Ni_{22}Mn_3Al_{20}$ rod at 10 K is about 196 A m^2/kg, which is higher than that of the $Gd_{55}Ni_{25}Al_{20}$ as-cast rod (about 187 A m^2/kg). The

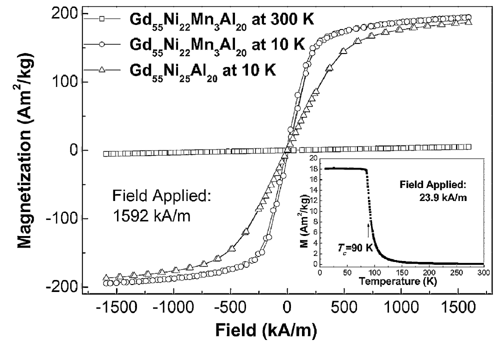

Fig. 2. Magnetic hysteresis loops of the $Gd_{55}Ni_{22}Mn_3Al_{20}$ as-cast rod at 300 K and 10 K, and the $Gd_{55}Ni_{25}Al_{20}$ as-cast rod at 10 K under a magnetic field of about 1592 kA/m, the inset the *M*–*T* curve of the $Gd_{55}Ni_{22}Mn_3Al_{20}$ glassy rod under the field of 23.9 kA/m from 10 K to 300 K.

higher M_s value of the $Gd_{55}Ni_{22}Mn_3Al_{20}$ as-cast rod indicates an enlarged total magnetic moment, suggesting an enhanced magnetic entropy change, ΔS_m due to the minor Mn addition. The temperature dependence of magnetization (*M*–*T* curve) under a field of 23.9 kA/m from 10 K to 300 K is shown in the inset of Fig. 2. The abrupt magnetization drop near the Curie temperature (T_c) of the BMG also suggests a higher ΔS_m of the $Gd_{55}Ni_{22}Mn_3Al_{20}$ BMG. The Curie temperature of the $Gd_{55}Ni_{22}Mn_3Al_{20}$ as-cast rod is about 90 K, which is higher than that of the $Gd_{55}Ni_{25}Al_{20}$ glassy rod (about 80 K). The higher value of T_c indicates a higher peak temperature of the magnetic entropy change.

Fig. 3 shows the isothermal magnetization curves (*M*–*H* curves) of the $Gd_{55}Ni_{22}Mn_3Al_{20}$ glassy rod, measured at temperatures ranging from 20 K to 160 K under a magnetic field of 3979 kA/m. By applying the thermodynamic Maxwell equation, the magnetic entropy changes of the $Gd_{55}Ni_{22}Mn_3Al_{20}$ glassy rod as a function of temperature ($(-\Delta S_m)$–T curve) can be obtained, as shown in Fig. 4(a). The BMG shows a typical broadened ΔS_m peak of ferromagnets with second order phase transition. The

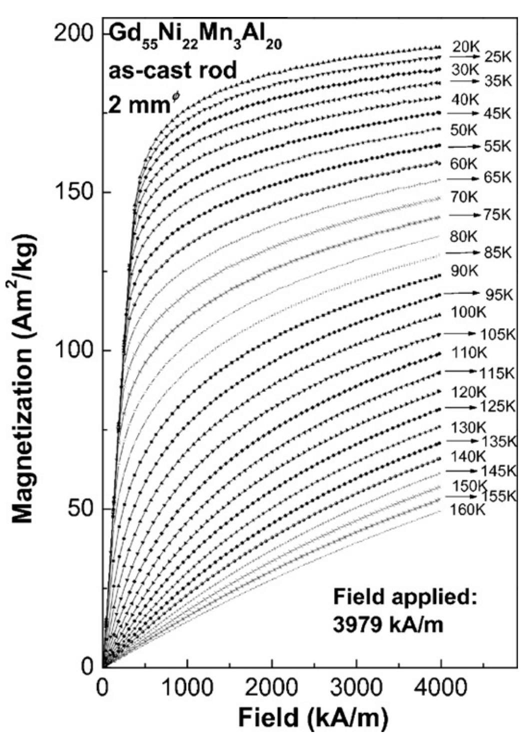

Fig. 3. Isothermal magnetization curves of $Gd_{55}Ni_{22}Mn_3Al_{20}$ as-cast rod under a magnetic field of 3979 kA/m.

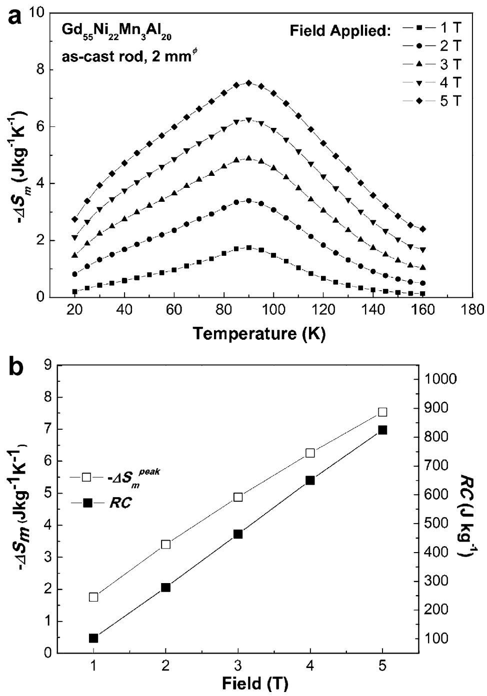

Fig. 4. (a) The $(-\Delta S_m)$–T curve; (b) $-\Delta S_m^{peak}$ as wall as *RC* of the $Gd_{55}Ni_{22}Mn_3Al_{20}$ amorphous rod under the field of 796 kA/m, 1592 kA/m, 2387 kA/m, 3183 kA/m and 3979 kA/m.

peak $-\Delta S_m$ values ($-\Delta S_m^{peak}$) of the as-cast $Gd_{55}Ni_{22}Mn_3Al_{20}$ rod under magnetic fields of 796 kA/m, 1592 kA/m, 2387 kA/m, 3183 kA/m and 3979 kA/m, as shown in Fig. 4(b), are about 1.76 J kg^{-1} K^{-1}, 3.40 J kg^{-1} K^{-1}, 4.88 J kg^{-1} K^{-1}, 6.25 J kg^{-1} K^{-1} and 7.54 J kg^{-1} K^{-1} at a temperature of 90 K, respectively. The $-\Delta S_m^{peak}$ of the $Gd_{55}Ni_{22}Mn_3Al_{20}$ as-cast rod is slightly lower but much broader than that of a $Gd_{55}Ni_{25}Al_{20}$ ternary BMG [15,17].

It should be noted that $-\Delta S_m^{peak}$ is not a unique parameter for evaluating the MCE of magnetic refrigerants, especially for ferromagnets with broadened but less intense $-\Delta S_m$ peak. The refrigerant capacity, defined as the amount of heat that can be transferred in one thermodynamic cycle, is a more important parameter for the evaluation of MCE from the technological point of view [21–23]. This parameter not only considers the $-\Delta S_m^{peak}$ of refrigerant materials, but also takes into account the shape of the $(-\Delta S_m)$–T curve. It should be noted that ferromagnets with first order phase transition, such as $Gd_5Si_2Ge_2$ and $Ni_2Mn_{1-x}Cu_xGa$, usually exhibit ΔT_m values lower than 30 K, even though they exhibit relative high $-\Delta S_m^{peak}$ values [21,27]. While amorphous samples, for example, $Gd_{55}Ni_{25}Al_{20}$ BMGs, show a much larger ΔT_m up to 70 K under a field of 2 T [15,17]. In present work, ΔT_m of the $Gd_{55}Ni_{22}Mn_3Al_{20}$ as-cast rod is about 58.5 K under 796 kA/m, 82 K under 1592 kA/m, 95 K under 2387 kA/m, 104 K under 3183 kA/m and 109.5 K under 3979 kA/m. ΔT_m of the $Gd_{55}Ni_{22}Mn_3Al_{20}$ as-cast rod is obviously enlarged by the minor Mn addition. As a result, associated with the $-\Delta S_m^{peak}$, the *RC* of a $Gd_{55}Al_{20}Ni_{22}Mn_3$ as-cast rod reaches about 103 J kg^{-1} under 796 kA/m, 279 J kg^{-1} under 1592 kA/m, 464 J kg^{-1} under 2387 kA/m, 650 J kg^{-1} under 3183 kA/m and 825 J kg^{-1} under 3979 kA/m, as shown in Fig. 4(b). The *RC* value of $Gd_{55}Ni_{22}Mn_3Al_{20}$ BMG is much larger than the pure Gd (517 J kg^{-1} under 5 T) [28,29] and for most of the other Gd-based amorphous alloys reported previously, such as $Gd_{55}Co_{20}Al_{25}$ BMG (541 J kg^{-1} under 5 T) [13,16,17], $Gd_{55}Ni_{25}Al_{20}$ BMG (622 J kg^{-1} under 5 T) [15,17], $Gd_{53}Al_{24}Co_{20}Zr_3$ BMG (590 J kg^{-1} under 5 T) [13], $Gd_{33}Er_{22}Al_{25}Co_{20}$ BMG (574 J kg^{-1} under 5 T) [13], $Gd_{32}Tb_{26}Al_{22}Co_{20}$ BMG (642 J kg^{-1} under 5 T) [19], $Gd_{71}Fe_3Al_{26}$ amorphous ribbon (750 J kg^{-1} under 5 T) and $Gd_{65}Fe_{20}Al_{15}$ amorphous ribbon (750 J kg^{-1} under 5 T) [20]; let alone the crystalline compounds such as $Gd_5Si_2Ge_2$ (305 J kg^{-1} under 5 T) [21,30], Gd_5Sn_4 (400 J kg^{-1} under 5 T) [31] due to their narrow MCE temperature range. The high *RC* value makes the $Gd_{55}Ni_{22}Mn_3Al_{20}$ BMG an attractive candidate for magnetic refrigerants.

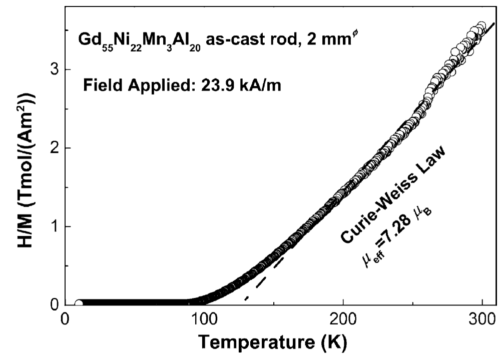

Fig. 5. Plot of ratio H/M as a function of temperature of $Gd_{55}Ni_{22}Mn_3Al_{20}$ as-cast rod under the field of 23.9 kA/m.

According to the above results, it is found that the replacement of Ni with small amount of Mn not only affects the $-\Delta S_m^{peak}$ value, but also increases ΔT_m dramatically, thus enhancing the *RC* of the BMG significantly. The broadened ΔT_m is usually regarded as a result of second order phase transition due to the disordered structure of amorphous alloys, while the enhanced *RC* value is supposed to be closely related to the enlarged magnetic moment of the BMG by micro-alloying. It is known that the MCE of a ferromagnetic material is commonly characterized by the entropy change in an isothermal process, and the entropy change is mainly caused by the reduced magnetic part of the total entropy due to the ordering of the magnetic moment under a magnetic field [24]. The increase of magnetic moment will definitely result in an enhanced *RC* value in a sample. The magnetic moment of a $Gd_{55}Ni_{22}Mn_3Al_{20}$ glassy rod is found to be about 6.56μ_B, which is higher than that of the $Gd_{55}Ni_{25}Al_{20}$ BMG (about 6.46μ_B). It could be the reason for the enlarged M_s and *RC* of BMGs by the minor Mn addition. A more useful way to evaluate the magnetic moment of the $Gd_{55}Ni_{22}Mn_3Al_{20}$ amorphous alloy is to calculate the effective magnetic moment (μ_{eff}) from the temperature dependence of H/M of the BMG according to the Curie–Weiss law. A plot of the ratio H/M as a function of temperature (H/M–T curve) under the a field of 23.9 kA/m is shown in Fig. 5. The μ_{eff} of the $Gd_{55}Ni_{22}Mn_3Al_{20}$ BMG, as shown in Fig. 5, is about 7.28μ_B, and is also larger than that of a $Gd_{55}Ni_{25}Al_{20}$ BMG (about 7.2μ_B obtained from the M–T curve of $Gd_{55}Ni_{25}Al_{20}$ BMG under 79.6 kA/m [15]). The higher *RC* value of the $Gd_{55}Ni_{22}Mn_3Al_{20}$ BMG compared to that of a $Gd_{55}Ni_{25}Al_{20}$ BMG is likely due to the higher μ_{eff} value. The relatively high value of μ_{eff} of the $Gd_{55}Ni_{22}Mn_3Al_{20,}$ which is much closer to that of a Gd^{3+} ion (7.94μ_B) can be attributed to the strong interaction of the magnetic moment between the rare-earth element with 4*f*-electrons and the transition metal element with 3*d*-electrons.

4. Conclusion

A $Gd_{55}Ni_{22}Mn_3Al_{20}$ BMG with excellent GFA and MCE was synthesized by copper mold casting through the minor substitution of Ni with Mn in a $Gd_{55}Ni_{25}Al_{20}$ glass forming alloy. It was found that the ΔT, T_{rg}, γ and Z_c values of the $Gd_{55}Ni_{22}Mn_3Al_{20}$ glassy rod are larger than those of $Gd_{55}Al_{20}Ni_{25}$ BMG, revealing the improved GFA and thermal stability through this minor Mn addition. Magnetic measurements at different temperatures have illustrated a higher M_s of the $Gd_{55}Ni_{22}Mn_3Al_{20}$ (about 196 A m^2/kg) than that of a $Gd_{55}Al_{20}Ni_{25}$ BMG (about 187 A m^2/kg) under the same magnetic field of 1592 kA/m. The $(-\Delta S_m)$–T curve derived from the isothermal M–H curves further reveals that the minor Mn addition does not only affect the $-\Delta S_m^{peak}$ value, but also increases ΔT_m dramatically, resulting in the enhancement of the RC of the $Gd_{55}Ni_{22}Mn_3Al_{20}$ BMG. The RC of the $Gd_{55}Ni_{22}Mn_3Al_{20}$ BMG is found to be about 825 J kg^{-1} under a field of 3979 kA/m, which is much higher than most of the other alloys reported previously. It is considered that the improvement is closely related to its large μ_{eff} (about 7.28μ_B) obtained from the H/M–T curve according to the Curie–Weiss law.

Acknowledgements

The work described in this paper was supported by The Hong Kong Polytechnic University under Project no. G-U721, and was partially supported by the National Nature Science Foundation of China under Grant no. 50731008.

References

[1] A.L. Greer, Science 267 (1995) 1947–1953.
[2] W.L. Johnson, MRS Bull. 24 (1999) 42–56.
[3] A. Inoue, T. Zhang, A. Takeuchi, Mater. Sci. Forum 269–272 (1998) 855–864.
[4] W.H. Wang, C. Dong, C.H. Shek, Mater. Sci. Eng. R 44 (2004) 45–89.
[5] H.J. Fecht, Mater. Trans. JIM 36 (1995) 777–793.
[6] H. Men, S.J. Pang, T. Zhang, J. Mater. Res. 21 (2006) 958–961.
[7] L. Xia, S.T. Shan, D. Ding, Y.D. Dong, Intermetallics 15 (2007) 1046–1049.
[8] Y.H. Liu, G. Wang, R.J. Wang, D.Q. Zhao, M.X. Pan, W.H. Wang, Science 315 (2007) 1385–1388.
[9] A. Inoue, W. Zhang, T. Zhang, K. Kurosaka, Acta Mater. 49 (2001) 2645–2652.
[10] J. Das, M.B. Tang, K.B. Kim, R. Theissman, F. Baier, W.H. Wang, J. Eckert, Phys. Rev. Lett. 94 (2005) 205501.
[11] L. Si, J. Ding, Y. Li, B. Yao, H. Tan, Appl. Phys. A 75 (2002) 535–539.
[12] C.L. Jo, L. Xia, D. Ding, Y.D. Dong, Chin. Phys. Lett. 23 (2006) 672–674.
[13] Q. Luo, D.Q. Zhao, M.X. Pan, W.H. Wang, Appl. Phys. Lett. 89 (2006) 081914.
[14] L. Liang, X. Hui, Y. Wu, G.L. Chen, J. Alloys Compd. 457 (2008) 541–544.
[15] D. Ding, L. Xia, Z.H. Yu, Y.D. Dong, Chin. Phys. Lett. 25 (2008) 3414–3417.
[16] Q. Luo, D.Q. Zhao, M.X. Pan, W.H. Wang, Appl. Phys. Lett. 92 (2008) 011923.
[17] J. Du, Q. Zheng, Y.B. Li, Q. Zhang, D. Li, Z.D. Zhang, J. Appl. Phys. 103 (2008) 023918.
[18] S. Gorsse, B. Chevalier, G. Orveillon, Appl. Phys. Lett. 92 (2008) 122501.
[19] Y.S. Liu, J.C. Zhang, Y.Q. Wang, Y.Y. Zhu, Z.L. Yang, J. Chen, S.X. Cao, Appl. Phys. Lett. 94 (2009) 112507.
[20] Q.Y. Dong, B.G. Shen, J. Chen, J. Shen, F. Wang, H.W. Zhang, J.R. Sun, J. Appl. Phys. 105 (2009) 053908.
[21] V.K. Pecharsky, K.A. Gschneider, Phys. Rev. Lett. 78 (1997) 4494–4497.
[22] A.M. Tishin, Y.I. Spichkin, The Magnetocaloric Effect and its Applications, Institute of Physics Publishing Ltd., Bristol, 2003.
[23] K.A. Gschneider, V.K. Pecharsky, A.O. Tsokol, Rep. Prog. Phys. 68 (2005) 1479–1539.
[24] N.A. de Oliveira, P.J. von Ranke, Phys. Rep. 489 (2010) 89–159.
[25] W.H. Wang, Prog. Mater. Sci. 52 (2007) 540–596.
[26] A. Inoue, Acta Mater. 48 (2000) 279–306.
[27] F.X. Hu, B.G. Shen, J.R. Sun, G.H. Wu, Phys. Rev. B 64 (2001) 132412.
[28] V.K. Pecharsky, K.A. Gschneider, J. Magn. Magn. Mater. 200 (1999) 44–56.
[29] A. Fujita, S. Fujieda, Y. Hasegawa, K. Fukamichi, Phys. Rev. B 67 (2003) 104416.
[30] V. Provenzano, A.J. Shapiro, R.D. Shull, Nature 429 (2004) 853–857.
[31] D.H. Ryan, M. Elouneg-Jamroz, J. van Lierop, Z. Altounian, H.B. Wang, Phys. Rev. Lett. 90 (2003) 117202.